Title
Competitive Incorporation of Perrhenate and Nitrate into Sodalite

Journal
Environmental Science, 48(21)

ISSN
0013-936X

Authors
Dickson, Johnbull O.
Harsh, James B.
Flury, Markus
et al.

Publication Date
2014-11-04

Competitive Incorporation of Perrhenate and Nitrate into Sodalite

Johnbull O. Dickson [a], James B. Harsh [a], Markus Flury [a], Wayne W. Lukens [b], and Eric M. Pierce [c]*

[a]Department of Crops and Soil Sciences, Washington State University, P. O. Box 646420, Pullman, WA 99164, USA

[b]Chemical Sciences Division, Lawrence Berkeley National Laboratory, Berkeley, CA 94720

[c]Environmental Sciences Division, Oak Ridge National Laboratory, P. O. Box 2008, Oak Ridge, TN 37831.

*Corresponding Author:

Johnbull Dickson

Department of Crop and Soil Sciences

Washington State University

P. O. Box 646420

Pullman, WA 99164

Phone: +1-509-335-3475

Fax: +1-509-335-8674

Email: j.dickson@wsu.edu

ABSTRACT

Nuclear waste storage tanks at the Hanford site in southeastern Washington have released highly alkaline solutions, containing radioactive and other contaminants, into subsurface sediments. When this waste reacts with subsurface sediments, feldspathoid minerals (sodalite, cancrinite) can form, sequestering pertechnetate ($^{99}TcO_4^-$) and other ions. This study investigates the potential for incorporation of perrhenate (ReO_4^-), a chemical surrogate for $^{99}TcO_4^-$, into mixed perrhenate/nitrate (ReO_4^-/NO_3^-) sodalite. Mixed-anion sodalites were hydrothermally synthesized in the laboratory from zeolite A in sodium hydroxide, nitrate, and perrhenate solutions at 90 °C for 24 to 168 hours. The resulting solids were characterized by bulk chemical analysis, X-ray diffraction, scanning electron microscopy, and X-ray absorption near edge structure spectroscopy (XANES) to determine the products' chemical composition, structure, morphology, and Re oxidation state. The XANES data indicated that nearly all rhenium (Re) was incorporated as $Re(VII)O_4^-$. The non-linear increase of the unit cell parameter with higher ReO_4^-/NO_3^- ratios suggests formation of two separate sodalite phases in lieu of a mixed-anion sodalite. The results reveal that the sodalite cage is highly selective towards the NO_3^- over ReO_4^-. Calculated enthalpy and Gibbs free energy of formation at 298 K for NO_3- and ReO_4-sodalite suggest that NO_3^- incorporation into the cage is favored over the incorporation of the larger ReO_4^-, due to the smaller ionic radius of NO_3^-. Based on these results, it is expected that NO_3^-, which is present at significantly higher concentrations in alkaline waste solutions than $^{99}TcO_4^-$, will be strongly preferred for incorporation into the sodalite cage.

■ INTRODUCTION

Technetium-99 presents a major environmental concern due to its long half-life (211,000 y) and high mobility of pertechnetate (TcO_4^-), the dominant ionic species in oxidized subsurface systems. [1] At the U.S. Department of Energy's Hanford Site, approximately 1900 kg of ^{99}Tc was generated and stored underground in 177 tanks, which contain an estimated 65 million gallons of nuclear waste from the production of plutonium during the Cold War era. [2] Seventy-seven of these tanks have leaked high-level radioactive waste (HLW) into the vadose zone (the unsaturated region which extends from the ground surface to the top of the water table), which extends 50 to 70 meters below the storage tanks. [2] In addition ^{99}Tc was also released to the subsurface via cribs and trenches, which received in excess of 50 million gallons of reprocessed tank waste. Due to weak adsorption of TcO_4^- to the predominantly negatively-charged, oxic sediments prevalent at the Hanford site, ^{99}Tc migration into the vadose zone water and groundwater is expected to be largely unimpeded. [3]

The Hanford tank waste solutions are alkaline (free OH^- is from 0.1 to 5.3 M, Na^+ from 2.9 to 19.6 M, and NO_3^- from 0.5 to 5.5 M), high in ionic strength (I = 2 – 14), and supersaturated with an $Al(OH)_3$ phase. [3-6] The tanks contain several radionuclides and contaminants of concern, including NO_3^-, CrO_4^{2-}, $^{137}Cs^+$, $^{90}Sr^{2+}$, TcO_4^-, and $^{79}SeO_4^{2-}$ that have been detected in groundwater. Model simulations of ^{99}Tc transport in the vadose zone suggest that the groundwater concentrations beneath the cribs and trenches in the central plateau should be in excess of the maximum allowable contaminant level of 0.4 nmol L^{-1} [7]. Interestingly, nearly 50 years after being released, ^{99}Tc data from borehole soil/sediment samples collected at varying depths within the central plateau of the Hanford site indicate that a significant portion of ^{99}Tc is present in a relatively immobile form. [8] The reduction of TcO_4^- to immobile TcO_2 [Tc(IV)] by Fe(II)-bearing minerals present in the vadose zone has been proposed to explain this observation.[9, 10] Alternatively, $^{99}TcO_4^-$ may be intercalated into feldspathoid phases.

Previous laboratory studies have shown that when simulated tank leachate reacts with native Hanford sediments, the primary and secondary (alumino) silicate minerals react with leachate to form precipitates including allophane, zeolite, and feldspathoids (e.g., sodalite, cancrinite).[11-14] These investigations demonstrated that, among the feldspathoids, sodalite—$[Na_8(Al_6Si_6O_{24})(NO_3)_2]$—incorporates ^{90}Sr and ^{137}Cs from HLW, by replacing Na in the structure.[15, 16]

Cancrinite and sodalite share the same formula (identical stoichiometry), however the spatial arrangement of their framework structures is different. Feldspathoid minerals have a three-dimensional, oxygen-tetrahedral framework containing Al and Si in a network system with multiple channels, cages and pores.[17, 18] A typical feldspathoid is represented by the general formula $M_8(Al_6Si_6O_{24})X_2$, where M is a metal cation—e.g. Cs, K, Na,—and X is an anion—such as Cl^-, NO_3^-, TcO_4^-, ReO_4^-, or SO_4^{2-}.[17] Sodalite consists of alternating TO_4 corner-sharing tetrahedra (where T is usually Si or Al) forming four and six ring cages, which make up the so-called β-cage or a sodalite cage. In the Cl-bearing sodalite, these cages are approximately 6.5 Å in diameter and are accessible through 2.6 Å-wide six-membered rings that form continuous channels for diffusion of intra-framework ions.[19-21] The six-membered ring is occupied by four cations tetrahedrally associated with an anion (e.g., Cl^-) at the center of the cage. With the exception of hydroxide, anions are irreversibly trapped within the cages, and once cages have formed it becomes difficult to replace anions without destroying the cage. [22]

The role of feldspathoids in attenuating the migration of anionic forms of radionuclides and contaminants of concern remains an open and critical question. The incorporation of TcO_4^- into sodalite may play an important role in waste containment below the Hanford waste tanks. Therefore, we examined (1) the formation of sodalite in the presence of NO_3^- and ReO_4^- anions, (2) the oxyanion selectivity, and (3) the relationship between ReO_4^-/NO_3^- concentration in the solid and anion/cage size. The objective was to quantify the extent of ReO_4^- incorporation into mixed perrhenate/nitrate sodalite as

a function of anion composition. The various points of interest were examined by hydrothermal reaction at 90°C for 24 h using Na^+, OH^-, and NO_3^- concentrations in solutions similar to those found in the Hanford waste tanks, while supplying Si and Al from a zeolite solid phase. Perrhenate serves as a viable surrogate for ^{99}Tc because both elements occur under oxidizing conditions as oxyanions (ReO_4^- and TcO_4^-), and have similar metal oxygen bond lengths (Tc–O = 1.702 Å and Re–O = 1.719 Å) and ionic radii (TcO_4^- = 2.52 Å and ReO_4^- = 2.60 Å).[23-25] Because the standard electrode potentials of the two species differ (ReO_4^-/ReO_2 = 0.510 V and TcO_4^-/TcO_2 = 0.738 V) [26, 27], this study only considers the behavior of the oxidized species, the expected stable form in the Hanford vadose zone. Results of this study will clarify the role of feldspathoids in the long-term fate and transport of $^{99}TcO_4^-$ below the Hanford tanks, and, ultimately, will help manage waste containment.

■ EXPERIMENTAL METHODS

Hydrothermal Synthesis. The ReO_4^-/NO_3^- sodalites were hydrothermally synthesized at 90°C for 24 h from zeolite 4A using the following modification of a method described by Liu et al., [28]:

Mixed sodalites were synthesized in a 60-mL Teflon® digestion bombs, filled with 20 mL of de-ionized water, 1 g of NaOH pellets and 0.5 g of zeolite 4A. While keeping the total molarity constant (1.77 *M*), different molar ratios of $NaNO_3$ and $NaReO_4$ (0.25 to 9.0 NO_3^-/ ReO_4^-) were added to the basic solutions. All chemical reagents were used as received. The bombs were capped, agitated and heated at 90 °C in an oven for 24 h. The temperature used was in line with the temperatures near or greater than the 100 °C reported within and below the Hanford tanks.[29, 30]The supernatant solutions were decanted and the solid precipitates washed three times with deionized water (0.054×10^{-3} dS/m) by centrifugation at 17,000 rcf. The white solids were dried at 70 ^{0}C for 24 hours, weighed and dialyzed against deionized water until the electrolytic conductivity was ≤0.01 dS/m. Typical dialyzed solid yield was 0.5 – 0.6 g. At either 80 or 90 °C zeolite 4A was completely transformed into sodalite with minor

amount of cancrinite in 24 h, while below 70 °C no significant amount of sodalite was observed (data not shown). Sodalite formed at 80^0C incorporated Re at the same level as the 90^0C samples. The conditions for the hydrothermal synthesis are summarized in Table 1.

Characterization.

Powder X-ray Diffraction. X-ray diffraction (XRD) patterns were used for phase identification, morphological composition (phase purity), and structural analysis. Samples were hand crushed by mortar and pestle, evenly smeared on zero-background Si holders, and characterized by one of the following instruments: (1) Panalytical Xpert diffractometer (XRD) scanning at 0.02° steps and at a rate of 1.5°/min over 5 – 90° 2θ using MoKα radiation (λ = 0.709319 Å) with X'Celerator detector equipped with either ¼° fixed divergence slits and/or ½° anti-scatter slit. (2) Siemens diffractometer (D500 XRD) scanning at 0.05° steps over 5 – 90° 2θ using Ni-filtered CuKα radiation (λ = 1.54050 Å) and a graphite monochromator equipped with a scintillator detector.

Both X-ray diffractometers used radiation generated at 35 - 40 keV and 30 – 40 mA and a 5 – 10 s dwell time at each step. A mineral search match was conducted using "Jade" and/or HighScore software and the ICDD database. Rietveld refinements of crystallographic data of powder samples were performed using GSAS with EXPGUI interface and/or HighScore software packages[31] by varying the detector background, unit cell, Na position, N/Re occupancy, peak shape (U, V, W, and two other peak shapes), overall thermal parameter (B), and preferred orientation. These phases—$[Na_8(AlSiO_4)_6(NO_2)_2]$ [32], $[Na_8(AlSiO_4)_6(ReO_4)_2]$ [33], and $[Na_6Ca_{1.5}(AlSiO_4)_6(CO_3)_{1.5}(H_2O)_{1.75}]$ [34]—were used as reference structures for the refinement.

X-ray Absorption Near Edge Structure (XANES) Spectroscopy. Sodalite samples, consisting of powdered sodalite mixed with boron nitride were mounted on an aluminum holder with Kapton windows. XANES measurements were performed at the Stanford Synchrotron Radiation Lightsource

(SSRL) at the 11-2 beamline by using the Si (220) double crystal monochromator (ϕ = 90 crystals), detuned 50% to reduce the harmonic content of the beam. Spectra were collected from 0.2 keV below to 10 keV above the Re L_2-edge (11.959 keV). Data were either collected in transmission mode using nitrogen-filled ion chambers or fluorescence mode using a 100-element Ge detector and were corrected for detector dead time. Data were reduced from raw data to spectra using SixPack and normalized using Artemis.[35] Normalized XANES spectra were fit using standard spectra in the locally written program 'fites', which utilizes a non-linear least squares fitting data. Reference spectra from two standard samples, ReO_2(s) (Alfa–Aesar) and pure ReO_4-sodalite,[33] were used for data fitting. The sample XANES spectra were allowed to vary in energy during fitting and the spectral resolution is 7 eV based on the width of the white line at the Re L_2-edge.

Electron Microscopy. Scanning electron micrographs were obtained by sputter-coating powder samples with platinum-palladium to 2-nm thickness. Powder samples were subsequently examined under a field emission scanning electron microscope (FESEM) equipped with a field emission gun (FEI Quanta 200F, FEI Co., Hillsboro, OR) and Everhart-Thornley detector. The FESEM has an accelerating voltage of 30 keV with a resolution of 1 nm.

Chemical Digestion. Dialyzed powder samples were digested in 3% nitric acid and analyzed for Na concentration by atomic emission and/or absorption spectrophotometry (Varian 220 Flame Atomic Absorption Spectrometer, Varian Ltd., Mulgrave, Australia) and for Si and Al colorimetrically by the silicomolybdous acid method and 8-hydroxyquinoline-butyl acetate method respectively [36, 37]. Chemical composition of the solid for Re was analyzed by inductively coupled plasma-mass spectrometer (Agilent 7700 ICP-MS). Concentration of NO_3^- was determined by flow injection analysis using the QuikChem 8000 series (Lachat Instruments, Inc., Milwaukee, WI).

■ RESULTS

Structure of Mixed Sodalite. The refined powder XRD patterns of the pure and mixed-anion sodalites are displayed in Figure 1. Based on the refinement data, a small amount of cancrinite (~10 weight % on average) is formed along with the pure and mixed sodalite. For the mixed sodalites, predominance of well-defined X-ray diffraction peaks consistent with the $P\bar{4}3n$ space group and other minor peaks belonging to cancrinite ($P6_3$ space group) were observed. Cancrinite is characterized by a systematic absence of X-ray diffraction for 0,0,*l* reflections where *l* = odd, while sodalite lacks systematic diffraction peaks for *h,k,l* reflections where *h*+*k*+*l* = odd [32, 38]. The main distinguishing diffraction peaks for cancrinite correspond to the (101) and (211) Miller indices with *d*-spacings of ≈4.67 Å and 3.24 Å, respectively. The X-ray diffraction pattern for the sodalite phases indicate either pure or a mixed-anion phases. For the pure phase sodalites, the (211) diffraction peak of the pure NO_3-sodalite shifted from a higher 2θ (24.3°) to a lower 2θ (23.8°) for the ReO_4-sodalite end-member consistent with larger ionic radius of ReO_4^-. Lattice and refinement parameters for both the pure and mixed sodalites are shown in Table 1. Based on the Rietveld refinements, the space group $P\bar{4}3n$ and lattice parameters: *a* = 8.9762 Å, 9.1532 Å were adopted for the pure NO_3- and ReO_4-sodalites respectively. The space group $P6_3$ and the calculated lattice parameters: *a* = 12.683 Å and *c* = 5.1827 Å were assigned to the minor phase NO_3-cancrinite. [39, 40] For the mixed ReO_4/NO_3-sodalites, the refined cell parameters ranged from 8.9808 to 8.9987 Å, while at higher weight fractions of ReO_4^- in the mixed sodalite lattice the refined cell parameters varied from 9.1406 to 9.1457 Å.

The XANES data for select mixed sodalites were fit using only the spectra of ReO_2 and perrhenate sodalite. The fit results are presented in Table S1, and the spectra of the SOD-40 sample along with the reference spectra used in the fitting are displayed in Figure 2. In all cases, the spectrum of ReO_4-sodalite contributes significantly to the fit with insignificant contribution from the spectrum of ReO_2. The upper

limit of ReO_2 in the solid phase is twice the standard deviation – 12%. These data confirm that the Re in the formed solids occurred almost entirely as $Re(VII)O_4^-$.

Morphology of Synthesis Product. The SEM images indicate no morphological differences among the mixed sodalites. The morphology of the powder samples formed in the presence of either ReO_4^- or NO_3^- and varying ReO_4^-/NO_3^- ratio in solution was mostly lepispheric and/or lenticular-shaped structures, comprised of inter-grown thin disks or blades (Figure 3A-D). Similarly, Deng et al.,[16] using a starting Na-silicate and -aluminate solution with Si/Al <1.4, reported similar morphology during hydrothermal synthesis of sodalite co-crystallized with cancrinite.

Chemical Composition. The chemical composition of the synthesis products obtained from chemical digestion is shown in Table 2. All elements were assigned to sodalite based on the observation that only sodalite and a small amount of cancrinite were detected by XRD, and sodalite and cancrinite share the same chemical formula $[M_8(Al_6Si_6O_{24})X_2]$; the XRD peaks for cancrinite are consistent with a pure NO_3-cancrinite phase; and the amount of ReO_2 detected by XANES was negligible. The pure ReO_4- and NO_3-sodalite phases contained 1.94 and 1.99 mol of ReO_4^- and NO_3^-, respectively, per formula unit in agreement with the ideal value of 2.00. The mixed sodalite contained from 0.01 – 0.14 mol of ReO_4^-, much lower than its concentration relative to NO_3^- in solution. In general, ~0.1 – 2.1% of the ReO_4^- in the synthesis solution was incorporated into the mixed sodalite. Thus, the mixed sodalites were dominated by the NO_3-sodalite phase.

■ DISCUSSION

Effect of Anion Type. The type of anion present in the synthesis solutions containing a 1:1 molar ratio of Si/Al significantly affects the formation pathway of the mixed ReO_4/NO_3-sodalite. Deng et al.,[41] reported that Cl^- and NO_2^- predominantly favor the formation of sodalite over cancrinite whereas NO_3^-, CO_3^{2-}, and SO_4^{2-} foster cancrinite formation [41]. In our study of the mixed ReO_4- and NO_3-sodalites,

cancrinite was a minor phase and there was a strong preference for NO_3^- in the dominant sodalite phase. The primary difference in the synthesis procedures was the use of zeolite A as a 1:1 Si/Al source while Deng et al. used various Si/Al ratios from dissolved species.

Competitive Incorporation of NO_3^- and ReO_4^- into Mixed Sodalite. The results showed that the NO_3-sodalite phase was dominant even when the solution mole fraction of ReO_4^- was 0.80. The competitive advantage of NO_3^- over ReO_4^- could be due to two major factors: (1) an entropic advantage of placing the smaller anion in the cage or (2) an enthalpic gain associated with the anion effect on cage size. Based on the results discussed in Pierce et al. (in review), [42] the difference in the Gibbs free energies of the two solid phases is largely explained by the difference in enthalpies suggesting that the larger cage size (Table 1) imposed by the ReO_4^- ion (ionic radius = 2.60 Å) is unfavorable in comparison with that imposed by the NO_3^- (ionic radius = 1.96A). A similar argument was made by Trill et al.,[43] with regard to sodalite favoring Cl^- over I^-. The findings in this study suggest that the formation of mixed sodalite at 90°C is modulated by enthalpy requirements due to the different sizes of the sodalite cages.

The competition of ReO_4^- and NO_3^- for the sodalite lattice can be written as follows:

$$(\mathrm{ReO_4^-})_s + (\mathrm{NO_3^-})_{aq} \underset{K_{NO_3}}{\overset{K_{ReO_4}}{\rightleftharpoons}} (\mathrm{ReO_4^-})_{aq} + (\mathrm{NO_3^-})_s \qquad (1)$$

where *aq* and *s* refer to the aqueous and solid phases, respectively. A selectivity coefficient can be defined as:

$$K_{ReO_4^-/NO_3^-} = \frac{M_{NO_3^-(s)}}{M_{ReO_4^-(s)}} \cdot \frac{M_{ReO_4^-(aq)}}{M_{NO_3^-(aq)}}$$

Herein $M_{ReO_4^-(aq)} = \frac{[ReO_4^-]_{aq}}{[ReO_4^-]_{aq}+[NO_3^-]_{aq}}$ and $M_{NO_3^-(aq)} = \frac{[NO_3^-]_{aq}}{[ReO_4^-]_{aq}+[NO_3^-]_{aq}}$ denote the mole fraction of perrhenate and nitrate in aqueous solutions and $K_{ReO_4^-/NO_3^-}$ the selectivity of sodalite for ReO_4^- over NO_3^-.

The $K_{ReO_4^-/NO_3^-}$ significantly increased from 0.09 to 0.98 with increasing mole fraction of ReO_4^- occluded in the sodalite phase. Increasing selectivity was found for the NO_3-sodalite as ReO_4^- mole fraction in solution approaches 0.9, above which incorporation of ReO_4^- into the mixed sodalite becomes significant.

This result is consistent with the hypothesis that the larger cage size required for ReO_4^- incorporation is responsible for the favored formation of NO_3-sodalite. In order to randomly incorporate ReO_4^- into the crystal structure of sodalite, it would be necessary to enlarge random sodalite cages where the smaller and favored cages were dominant resulting in significant distortion of the crystal structure. Presumably, the selectivity begins to increase significantly when enough ReO_4^- is incorporated to form sodalite domains with the larger cages. To test this hypothesis, we related the change in lattice parameter with increasing ReO_4^- concentration in the sodalite phase (Figure 4). According to Vegard's Rule [$a_{AB} = a_A(M_A) + (1\text{-}M_A)a_B$], formation of an ideal solid solution should result in a linear dependence of the lattice parameter (a_{AB}) on mole fraction (M_A, 1-M_A) and ion size of the constituent elements *A* and *B*.[43] The linear relationship observed for our system up to 0.8 mole fraction of ReO_4^- in solution (0.07 mole fraction of ReO_4^- in solid) implies the formation of a solid solution, not a discrete ReO_4-sodalite phase (Figure 5). At higher ReO_4^- mole fraction in the mixed sodalite ($M_{ReO_4^-(s)}$ >0.07) the dependence of the lattice parameter on ReO_4^- in the solid become nonlinear, indicating that ReO_4^- is not incorporated homogeneously (Figure 4). This is confirmed by the splitting of the (211) diffraction peak of the mixed sodalite observed in the powder XRD patterns (Figure S1).

Although Vegard's Rule is an empirical relation, the significant increase of ReO_4^- in the solid with higher ReO_4^- concentration in solution shown in Figure 5 implies that ReO_4^- is not homogeneously distributed within the mixed sodalite. This is not surprising given the large difference in calculated ionic radii of ReO_4^- and NO_3^-. We find it unlikely that ReO_4^- is incorporated into the cancrinite phase for the following reasons: (1) the refined cell parameter for cancrinite is within the expected value for the pure NO_3-cancrinite phase(s) reported in literature [39]; and (2) the cell parameter for sodalite increases with ReO_4^- incorporation.

Synthesis of mixed ReO_4/NO_3-sodalite over a range of ReO_4^-/NO_3^- in solution strongly favors the formation of the NO_3-sodalite phase(s). At ReO_4^- mole fractions in solution ≤ 0.9, NO_3^- incorporation is strongly favored, whereas at ≥ 0.9, ReO_4^- selectivity for the mixed sodalite becomes significantly enhanced.

Our findings are relevant to radioactive waste management at waste-impacted nuclear sites. The large preference for NO_3^- in the sodalite cages implies that formation of the smaller cage is favored in the sodalite framework; however, this study and others also demonstrate the feasibility of pure ReO_4-sodalite formation in the absence of NO_3^-.[33] For example results from recent study by Pierce et al.,[44] suggest that ReO_4^- and SO_4^{2-} were potentially incorporated into mixed-anion sodalite. Trill et al.,[45] also reported the synthesis of several guest-guest anion sodalites. These combined results suggest that feldspathoids can immobilize ^{99}Tc in the presence of other anions contained in the waste streams assuming their ionic radii are similar. Although the structure of feldspathoids allows for TcO_4^- incorporation into their frameworks [42], our results reveal that ReO_4^-, a surrogate for TcO_4^-, was significantly intercalated into sodalite only when small, competing anions such as NO_3^- are present in very low concentrations (ReO_4^-/NO_3^- ~30:1) or completely absent. Under the subsurface conditions

resulting from nuclear waste leaks or discharge, it is expected that NO_3^- anions with higher selectivity must be first exhausted prior to significant TcO_4^- incorporation into the sodalite structure.

■ ADDITIONAL CONTENT

Supporting Information. Additional information on XANES, SEM micrographs and ReO_4^- concentrations in solids are available free of charge via the Internet at http://pubs.acs.org

■ AUTHOR INFORMATION

Corresponding Author

*Tel.: +1-509-335-3475; fax: +1-509-335-8674; email: j.dickson@wsu.edu

Notes

The Authors declare no competing financial conflicts of interest

■ ACKNOWLEDGEMENTS

This material is based upon work supported by the U.S. Department of Energy (DOE), Office of Science, Biological and Environmental Research Program (SBER), and was performed at Washington State University under contract No. DE-PS02-09ER65075 and at Oak Ridge National Laboratory under contract No. DE-AC05-00OR22725. XANES analyses were supported by DOE, Office of Science, Basic Energy Sciences, Chemical Sciences, Biosciences, and Geosciences Division, Heavy Element Chemistry Program and were performed at Lawrence Berkeley National Laboratory under contract No. DE-AC02-05CH11231. XANES spectroscopy was performed at the Stanford Synchrotron Radiation Lightsource (SSRL), which is a DOE office of Science user facility operated by Stanford University. We

are also indebted to the staff at the Franceschi Microscopy and Imaging Center at Washington State University for access to and assistance with the use of their SEM facilities.

■ REFERENCES

1. Agnew, S. F.; Boyer, J.; R.A, C.; Duran, T. B.; FitzPatrick, J. R.; Jurgensen, K. A.; Ortiz, T. P.; Young, B. L. *Hanford chemical and radionuclide inventories: HDW Model*; LA-UR-96-3860; Los Alamos National Laboratory: Los Alamos, NM, 1997.

2. Gephart, R. E.; Lundgren, R. E. *Hanford Tank Cleanup: A Guide to understanding the Technical Issues*; Pacific Northwest National Laboratory: Richland, Washington, 1995.

3. Zachara, J. M.; Serne, J.; Freshley, M.; Mann, F.; Anderson, F.; Wood, M.; Jones, T.; Myers, D., Geochemical processes controlling migration of tank wastes in Hanford's vadose zone. *Vadose Zone Journal* **2007,** *6*, (4), 985-1003.

4. Lichtner, P. C.; Felmy, A. R., Estimation of Hanford SX tank waste compositions from historically derived inventories. *Computers & Geosciences* **2003,** *29*, (3), 371-383.

5. Mashal, K.; Harsh, J. B.; Flury, M.; Felmy, A. R.; Zhao, H. T., Colloid formation in Hanford sediments reacted with simulated tank waste. *Environ. Sci. Technol.* **2004,** *38*, (21), 5750-5756.

6. Golcar, G. R.; Colton, N. G.; Darab, J. G.; Smith, H. D. *Hanford tank waste simulants specification and their applicability for the retrieval, pretreatment, and vitrification processes*; BNFL-RPT-012; Pacific Northwest National Laboratory, Richland, Washington, 2000.

7. USDOE. *Vadose zone characterization project at the Hanford tank farms: AX tank farm report*; Pacific Northwest National Laboratory: Richland, Washington, 1997.

8. Serne, R. J.; Bjornstad, B. N.; Keller, J. M.; Thorne, P. D.; Lanigan, D. C.; Christensen, J. N.; Thomas, G. S. *Conceptual models for migration of key groundwater contaminants through the vadose zone and Into the unconfined aquifer below the B-complex*; PNNL-19277; Pacific Northwest National Laboratory: Richland, Washington, 2010; p 496.

9. Pearce, C. I.; Liu, J.; Baer, D. R.; Qafoku, O.; Heald, S. M.; Arenholz, E.; Grosz, A. E.; McKinley, J. P.; Resch, C. T.; Bowden, M. E.; Engelhard, M. H.; Rosso, K. M., Characterization of natural titanomagnetites ($Fe_{3-x}Ti_xO_4$) for studying heterogeneous electron transfer to Tc(VII) in the Hanford subsurface. *Geochim. Cosmochim. Acta* **2014,** *128*, 114-127.

10. Peretyazhko, T. S.; Zachara, J. M.; Kukkadapu, R. K.; Heald, S. M.; Kutnyakov, I. V.; Resch, C. T.; Arey, B. W.; Wang, C. M.; Kovarik, L.; Phillips, J. L.; Moore, D. A., Pertechnetate (TcO_4^-) reduction by reactive ferrous iron forms in naturally anoxic, redox transition zone sediments from the Hanford Site, USA. *Geochim. Cosmochim. Acta* **2012,** *92*, 48-66.

11. Qafoku, N. P.; Ainsworth, C. C.; Szecsody, J. E.; Qafoku, O. S., Transport-controlled kinetics of dissolution and precipitation in the sediments under alkaline and saline conditions. *Geochim. Cosmochim. Acta* **2004,** *68*, (14), 2981-2995.

12. Chorover, J.; Choi, S.; Rotenberg, P.; Serne, R. J.; Rivera, N.; Strepka, C.; Thompson, A.; Mueller, K. T.; O'Day, P. A., Silicon control of strontium and cesium partitioning in hydroxide-weathered sediments. *Geochim. Cosmochim. Acta* **2008,** *72*, (8), 2024-2047.

13. Qafoku, N. P.; Ainsworth, C. C.; Szecsody, J. E.; Qafoku, O. S., Aluminum effect on dissolution and precipitation under hyperalkaline conditions: I. Liquid phase transformations. *Journal of Environmental Quality* **2003,** *32*, (6), 2354-2363.

14. Qafoku, N. P.; Ainsworth, C. C.; Szecsody, J. E.; Bish, D. L.; Young, J. S.; McCready, D. E.; Qafoku, O. S., Aluminum effect on dissolution and precipitation under hyperalkaline conditions: II. Solid phase transformations. *Journal of Environmental Quality* **2003,** *32*, (6), 2364-2372.

15. Choi, S.; Chorover, J.; Bowers, G.; Strepka, C.; Mueller, K. T.; Rivera, N. A.; O'Day, P. A., GEOC 124-Characterization of Sr and Cs sequestration and mineral transformation from reaction of Hanford sediments and caustic waste. *Abstracts of Papers of the American Chemical Society* **2006,** *232*.

16. Deng, Y. J.; Flury, M.; Harsh, J. B.; Felmy, A. R.; Qafoku, O., Cancrinite and sodalite formation in the presence of cesium, potassium, magnesium, calcium and strontium in Hanford tank waste simulants. *Appl. Geochem.* **2006,** *21*, (12), 2049-2063.

17. Depmeier, W., The sodalite family - A simple but versatile framework structure. In *Micro- and Mesoporous Mineral Phases*, Ferraris, G.; Merlino, S., Eds. 2005; Vol. 57, pp 203-240.

18. Frising, T.; Leflaive, P., Extraframework cation distributions in X and Y faujasite zeolites: A review. *Microporous Mesoporous Mater.* **2008,** *114*, (1-3), 27-63.

19. Barrer, R. M.; Vaughan, D. E. W., Trapping of inert gases in sodalite and cancrinite crystals. *J. Phys. Chem. Solids* **1971,** *32*, (3), 731-743.

20. Fazal, T. High temperature studies of sodalites. A Thesis for the MRes in Materials Chemistry and Nanochemistry, University of Birmingham, 2011.

21. Missimer, D. M.; Rutherford, R. L. *Preparation and initial characterization of fluidized bed steam reforming pure-phase standards*; DE-AC09-08SR22470; Savannah River National Laboratory, Aiken, SC, 2013.

22. Acar, A. C.; Yucel, H.; Culfaz, A., The synthesis and sodium-silver ion exchange of sodalites. *Chem. Eng. Commun.* **2003,** *190*, (5-8), 861-882.

23. Marcus, Y., Thermodynamics of solvation of ions. Part 5 - Gibbs free energy of hydration at 298.15-K *Journal of the Chemical Society-Faraday Transactions* **1991,** *87*, (18), 2995-2999.

24. Moyer, B. A.; Bonnesen, P. V., *Physical Factors in Anion Separation. Supramolecular chemistry of anions*. Wiley-VCH, New York: 1979.

25. Icenhower, J. P.; Qafoku, N. P.; Zachara, J. M.; Martin, W. J., The biogeochemistry of Technetium: A review of the behavior of an artificial element in the natural environment. *American Journal of Science* **2010,** *310*, (8), 721-752.

26. Mendez, E.; Cerda, M. F.; Luna, A. M. C.; Zinola, C. F.; Kremer, C.; Martins, M. E., Electrochemical behavior of aqueous acid perrhenate-containing solutions on noble metals: critical review and new experimental evidence. *J. Colloid Interface Sci.* **2003,** *263*, (1), 119-132.

27. Schwochau, K., Technetium radiopharmaceuticals - Fundamentals, synthesis, structure, and development. *Angewandte Chemie-International Edition* **1994,** *33*, (22), 2258-2267.

28. Liu, Q.; Navrotsky, A., Synthesis of nitrate sodalite: An in situ scanning calorimetric study. *Geochim. Cosmochim. Acta* **2007,** *71*, (8), 2072-2078.

29. Pruess, K.; Yabusaki, S.; Steefel, C.; Lichtner, P., Fluid Flow, Heat Transfer, and Solute Transport at Nuclear Waste Storage Tanks in the Hanford Vadose Zone. *Vadose Zone Journal* **2002,** *1*, (1), 68-88.

30. Serne, R. J.; Lindenmeier, C. W.; Schaef, H. T., Geochemical conditions in the vadose zone at leaking single-shell tanks in the B-BX-BY waste management area in Hanford's 200 E area. *Abstracts of Papers of the American Chemical Society* **2001,** *222*, U492-U492.

31. Toby, B. H., EXPGUI, a graphical user interface for GSAS. *J. Appl. Crystallogr.* **2001,** *34*, 210-213.

32. Buhl, J. C.; Lons, J., Synthesis and crystal structure of nitrate enclathrated sodalite $Na_8(AlSiO_4)_6(NO_3)_2$. *J. Alloys Compd.* **1996,** *235*, (1), 41-47.

33. Mattigod, S. V.; McGrail, B. P.; McCread, D. E.; Wang, L. Q.; Parker, K. E.; Young, J. S., Synthesis and structure of perrhenate sodalite. *Microporous Mesoporous Mater.* **2006,** *91*, (1-3), 139-144.

34. Hackbarth, K.; Gesing, T. M.; Fechtelkord, M.; Stief, F.; Buhl, J. C., Synthesis and crystal structure of carbonate cancrinite $Na_8(AlSiO_4)_6CO_3 3.4H_2O$, grown under low-temperature hydrothermal conditions. *Microporous Mesoporous Mater.* **1999,** *30*, (2-3), 347-358.

35. Ravel, B.; Newville, M., Athena, Artemis, Hephaestus: Data analysis for X-ray absorption spectroscopy using Ifeffit. *Journal of Synchrotron Radiation* **2005,** *12*, 537-541.

36. Bloom, P. R.; Weaver, R. M.; McBride, M. B., The spectrophotometric and fluorometric determination of aluminum with 8 hydroxy quinoline and butyl acetate extraction *Soil Science Society of America Journal* **1978,** *42*, (5), 713-716.

37. Weaver, R. M.; Syers, J. K.; Jackson, L. M., Determination of silica in citrate-bicarbonate-dithionite extracts of soils. *Soil Science Society of America Journal* **1968,** *32*, 497-501.

38. Grundy, H. D.; Hassan, I., The crystal structure of a carbonate-rich cancrinite. *Can. Mineral.* **1982,** *20*, (May), 239-251.

39. Liu, Q.; Xu, H.; Navrotsky, A., Nitrate cancrinite: Synthesis, characterization, and determination of the enthalpy of formation. *Microporous Mesoporous Mater.* **2005,** *87*, (2), 146-152.

40. Buhl, J. C.; Stief, F.; Fechtelkord, M.; Gesing, T. M.; Taphorn, U.; Taake, C., Synthesis, X-ray diffraction and MAS NMR characteristics of nitrate cancrinite $Na_{7.6}$ $[AlSiO_4]_6(NO_3)_{1.6}(H_2O)_2$. *J. Alloys Compd.* **2000,** *305*, (1-2), 93-102.

41. Deng, Y. J.; Harsh, J. B.; Flury, M.; Young, J. S.; Boyle, J. S., Mineral formation during simulated leaks of Hanford waste tanks. *Appl. Geochem.* **2006,** *21*, (8), 1392-1409.

42. Pierce, E. M.; Lilova, K.; Lukens, W. W.; Navrotsky, A.; Fritts, J.; Rawn, C.; Jantzen, C. M.; Missimer, D. M.; Huq, A., Structure and thermochemistry of perrhenate sodalite and perrhenate/pertechnetate guest-guest sodalite. In *Proceeding of the national Academy of Science*, 2014, submitted.

43. Trill, H.; Eckert, H.; Srdanov, V. I., Topotactic transformations of sodalite cages: synthesis and NMR study of mixed salt-free and salt-bearing sodalites. *J. Am. Chem. Soc.* **2002,** *124*, (28), 8361-8370.

44. Pierce, E. M.; Lukens, W. W.; Fitts, J. P.; Jantzen, C. M.; Tang, G., Experimental determination of the speciation, partitioning, and release of perrhenate as a chemical surrogate for pertechnetate from a sodalite-bearing multiphase ceramic waste form. *Appl. Geochem.* **2014,** *42*, 47-59.

45. Trill, H.; Eckert, H.; Srdanov, V. I., Mixed halide sodalite solid solution systems. Hydrothermal synthesis and structural characterization by solid state NMR. *J. Phys. Chem. B* **2003,** *107*, (34), 8779-8788.

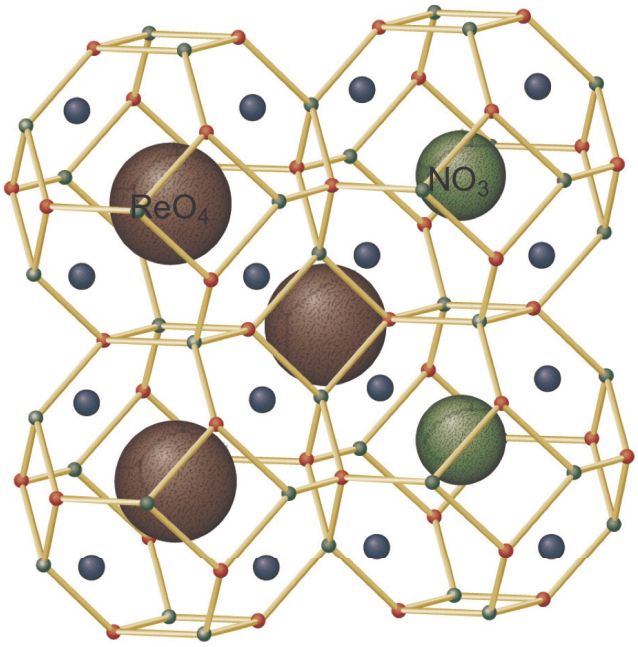

TOC/Abstract Art.

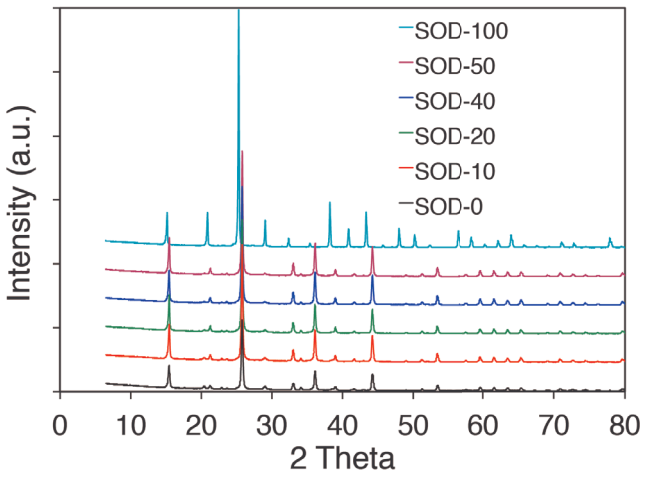

Figure 1. Refined powder X-ray spectra for selected mixed-anion and pure sodalite phases.

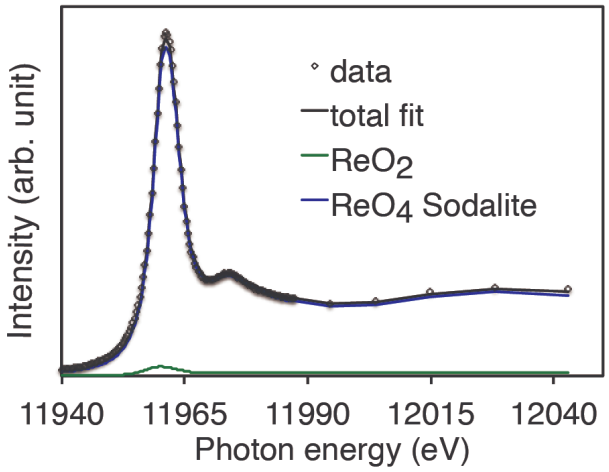

Figure 2. X-ray absorption spectral data of mixed sodalite (SOD-40 sample); Data are represented by dots, and the fit is shown by the black line. Results indicate Re(VII) oxidation state.

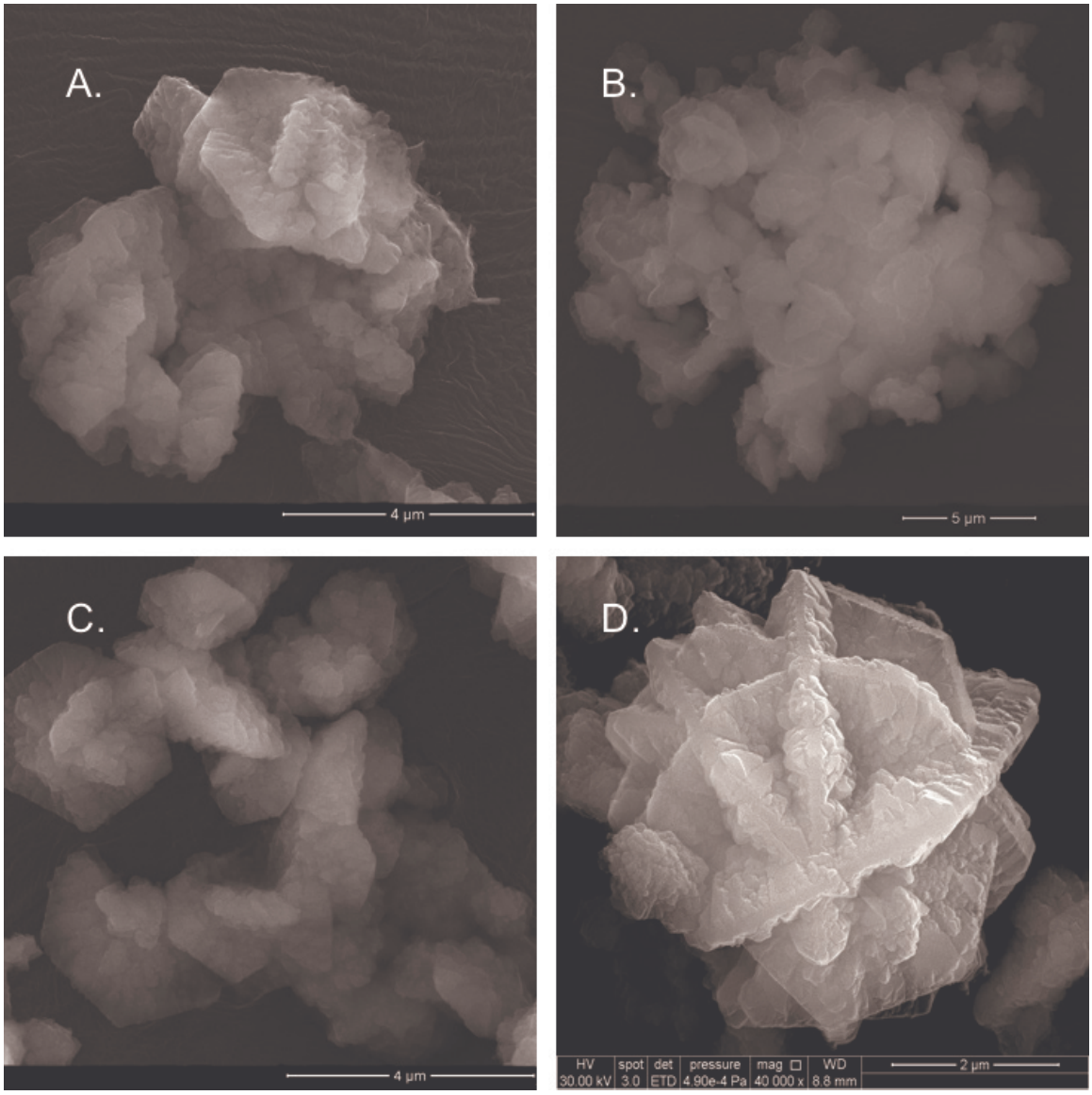

Figure 3. SEM images of ReO_4/NO_3-sodalites formed in varying ReO_4^-/NO_3^- molar ratio solutions.

"A" is SOD-10; "B" is -SOD-20; "C" is SOD-40; and "D" is SOD-50 samples

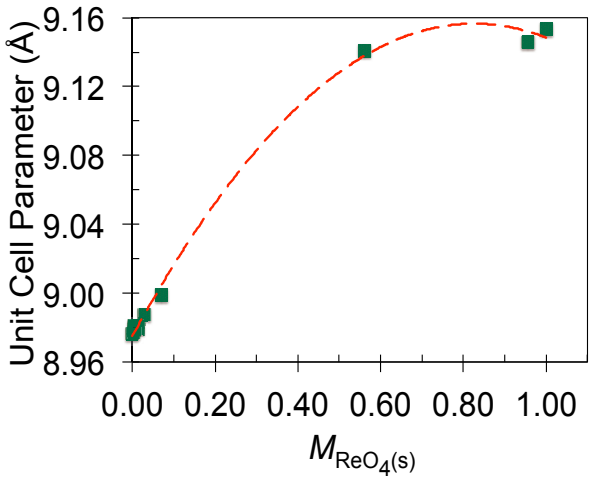

Figure 4. Dependence of the unit cell parameter on ReO_4^- concentration in ReO_4/NO_3-sodalite.

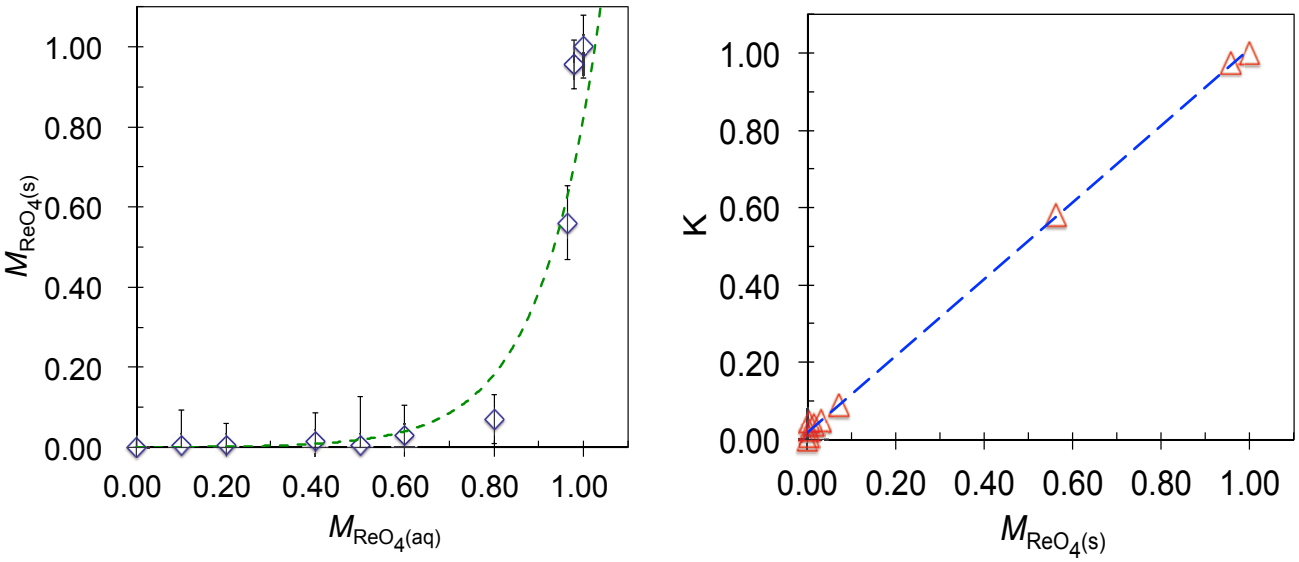

Figure 5. Selectivity graph (left) for rhenium incorporation into ReO_4/NO_3-sodalite; generally more than 90% of sodalite cages are filled with oxyanions. Selectivity coefficient (K) as a function of ReO_4^- mole fraction (right) in the mixed sodalite ($M_{ReO_4^-(s)}$).

Table 1. Conditions for the hydrothermal syntheses, and the refined X-ray data for mixed-anion sodalite

Sodalite type	Structural Formula	$NaReO_4$ (*M*)	$NaNO_3$ (*M*)	a	R_{wp}
SOD-0[‡]	$Na_8[Al_6Si_6O_{24}](NO_3)_{1.99}$	0	1.765	8.9762(3) [†]	10.38
SOD-10	$Na_8[Al_6Si_6O_{24}](ReO_{4(0.01)}NO_{3(2.09)})$	0.177	1.588	8.9808(3)	9.20
SOD-20	$Na_8[Al_6Si_6O_{24}](ReO_{4(0.01)}NO_{3(2.06)})$	0.353	1.412	8.9795(3)	12.36
SOD-40	$Na_8[Al_6Si_6O_{24}](ReO_{4(0.03)}NO_{3(1.97)})$	0.706	1.059	8.9774(3)	11.90
SOD-50	$Na_8[Al_6Si_6O_{24}](ReO_{4(0.01)}NO_{3(2.17)})$	0.883	0.883	8.9794(3)	12.18
SOD-60	$Na_8[Al_6Si_6O_{24}](ReO_{4(0.06)}NO_{3(1.94)})$	1.059	0.706	8.9873(3)	15.98
SOD-80	$Na_8[Al_6Si_6O_{24}](ReO_{4(0.14)}NO_{3(1.86)})$	1.412	0.353	8.9987(5)	11.07
SOD-96.5	$Na_8[Al_6Si_6O_{24}](ReO_{4(1.12)}NO_{3(0.88)})$	1.703	0.062	9.1406(7)	9.57
SOD-98	$Na_8[Al_6Si_6O_{24}](ReO_{4(1.91)}NO_{3(0.09)})$	1.730	0.035	9.1457(7)	14.55
SOD-100	$Na_8[Al_6Si_6O_{24}](ReO_4)_{1.94}$	1.765	0	9.1535(1)	9.09

[†]The number in parentheses is estimated standard deviation (esd) in the same decimal place as the digit preceding it. [‡]ReO_4^- mole fraction in the synthesis solution ($[ReO_4^-]/[ReO_4^-]+[NO_3^-]$) expressed in percentage; SOD-0 contains only NO_3^-; SOD-100 contains only ReO_4^-. The sodalite samples were synthesized at 90 °C for 24 h. "a" – lattice parameter, "R_{wp}" - weighted agreement factor.

Table 2. Chemical composition data for pure and mixed sodalite (mol/formula unit). Numbers are means and standard deviations of three replicates.

Formula of Structure	Na	Al	Si	ReO_4	NO_3
$Na_8[Al_6Si_6O_{24}](NO_3)_{1.99}$	7.91 ±0.06	6.00 ±0.08	6.15 ±0.23		1.99 ±0.03
$Na_8[Al_6Si_6O_{24}](ReO_{4(0.01)}NO_{3(2.09)})$	8.05 ±0.17	6.02 ±0.05	6.03 ±0.12	0.01	2.09 ±0.07
$Na_8[Al_6Si_6O_{24}](ReO_{4(0.01)}NO_{3(2.06)})$	8.05 ±0.17	6.02 ±0.05	6.03 ±0.12	0.01	2.06 ±0.03
$Na_8[Al_6Si_6O_{24}](ReO_{4(0.03)}NO_{3(1.97)})$	8.05 ±0.17	6.02 ±0.05	6.03 ±0.12	0.03	1.97 ±0.07
$Na_8[Al_6Si_6O_{24}](ReO_{4(0.01)}NO_{3(2.17)})$	8.05±0.17	6.02±0.05	6.03±0.12	0.01	2.17 ±0.02
$Na_8[Al_6Si_6O_{24}](ReO_{4(0.06)}NO_{3(1.94)})$	8.05±0.17	6.02±0.05	6.03±0.12	0.06	1.94 ±0.05
$Na_8[Al_6Si_6O_{24}](ReO_{4(0.14)}NO_{3(1.86)})$	8.05 ±0.17	6.02 ±0.05	6.03 ±0.12	0.14	1.86 ±0.01
$Na_8[Al_6Si_6O_{24}](ReO_{4(1.12)}NO_{3(0.88)})$	8.00 ±0.10	6.01 ±0.07	6.00 ±0.10	1.12 ±0.07	0.88 ±0.03
$Na_8[Al_6Si_6O_{24}](ReO_{4(1.91)}NO_{3(0.09)})$	7.95 ±0.09	5.98 ±0.09	6.05 ±0.07	1.91 ±0.06	0.09 ±0.02
$Na_8[Al_6Si_6O_{24}](ReO_4)_{1.94}$	8.00 ±0.20	5.97 ±0.04	6.09 ±0.09	1.94 ±0.03	

Supporting Information

Competitive Incorporation of Perrhenate and Nitrate into Sodalite

Johnbull O. Dickson[*1], *James B. Harsh*[1], *Markus Flury*[1], *Wayne W. Lukens*[2], *and Eric M. Pierce*[3]

[1]Department of Crops and Soil Sciences, Washington State University, P. O. Box 646420, Pullman, WA 99164, USA

[2]Chemical Sciences Division, Lawrence Berkeley National Laboratory, Berkeley, CA 94720

[3]Environmental Sciences Division, Oak Ridge National Laboratory, P. O. Box 2008, Oak Ridge, TN 37831.

*Corresponding Author: J.dickson@wsu.edu

Supporting information

- 3 pages (including cover page)
- 1 figure
- 1 table

*Corresponding Author: Tel.: +1-509-335-3475; fax: +1-509-335-8674;

Email: j.dickson@wsu.edu

This supplemental information contains additional information on XANES analysis

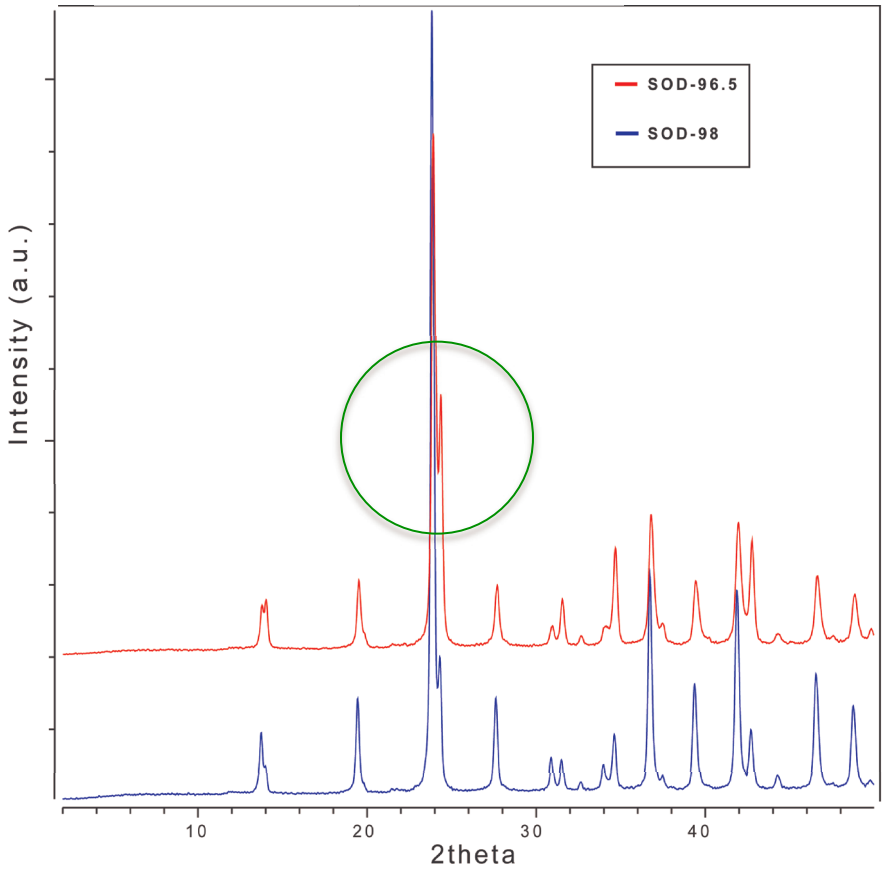

Figure S1. Refined powder X-ray spectra for mixed-anion sodalite. Shown within the circle is the splitting of the 211 diffraction peak indicative of two separate sodalite phases.

X-ray Absorption Near Edge Structure (XANES) Spectroscopy.

The spectra fitting were performed as previously described by Lukens et al. (2005, 2007) by inclusion of all reference spectra. Thus, the final fit includes only the reference spectra that have non-zero contributions to the fit. The improvement to the fit due to the contribution of the reference spectra was evaluated using the random error test (*F*-test), which is the likelihood that the improvement in the fit due to inclusion of the standard spectrum is due to noise in the data. If $p < 0.05$, then the data supports the hypothesis that a given component is present (improvement is > 2δ of the fit), and if $p < 0.01$, then the data strongly supports the hypothesis (improvement is > 3δ of the fit).

Table S1. Result of XANES spectra fitting for mixed ReO_4/NO_3-sodalite

Sample	ReO_2	p	ReO_4-sodalite	p
SOD-10	0.11(5)[†]	0.065	0.89(4)	<0.001
SOD-40	0.04(6)	0.560	0.96(4)	<0.001
SOD-50	0.05(6)	0.468	0.95(4)	<0.001

[†]The number in parentheses is the standard deviation in the same decimal place as the digit preceding it.

DISCLAIMER